J Arid Land (2023) 15(3): 274–296
https://doi.org/10.1007/s40333-023-0050-3

Science Press Springer-Verlag

Projection of precipitation extremes over South Asia from CMIP6 GCMs

Adnan ABBAS[1], Asher S BHATTI[2], Safi ULLAH[3], Waheed ULLAH[1], Muhammad WASEEM[4], ZHAO Chengyi[1*], DOU Xin[1], Gohar ALI[5]

[1] Land Science Research Center, Nanjing University of Information Science & Technology, Nanjing 210044, China;
[2] Department of Geology, Bacha Khan University, Charsadda 24420, Pakistan;
[3] Department of Atmospheric and Oceanic Sciences/Institute of Atmospheric Sciences, Fudan University, Shanghai 200438, China;
[4] Center of Excellence in Water Resources, University of Engineering and Technology, Lahore 54890, Pakistan;
[5] Pakistan Meteorological Department, Sector H-8/2, Islamabad 44000, Pakistan

Abstract: Extreme precipitation events are one of the most dangerous hydrometeorological disasters, often resulting in significant human and socio-economic losses worldwide. It is therefore important to use current global climate models to project future changes in precipitation extremes. The present study aims to assess the future changes in precipitation extremes over South Asia from the Coupled Model Intercomparison Project Phase 6 (CMIP6) Global Climate Models (GCMs). The results were derived using the modified Mann-Kendall test, Sen's slope estimator, student's *t*-test, and probability density function approach. Eight extreme precipitation indices were assessed, including wet days (RR1mm), heavy precipitation days (RR10mm), very heavy precipitation days (RR20mm), severe precipitation days (RR50mm), consecutive wet days (CWD), consecutive dry days (CDD), maximum 5-day precipitation amount (RX5day), and simple daily intensity index (SDII). The future changes were estimated in two time periods for the 21st century (i.e., near future (NF; 2021–2060) and far future (FF; 2061–2100)) under two Shared Socioeconomic Pathway (SSP) scenarios (SSP2-4.5 and SSP5-8.5). The results suggest increases in the frequency and intensity of extreme precipitation indices under the SSP5-8.5 scenario towards the end of the 21st century (2061–2100). Moreover, from the results of multimodel ensemble means (MMEMs), extreme precipitation indices of RR1mm, RR10mm, RR20mm, CWD, and SDII demonstrate remarkable increases in the FF period under the SSP5-8.5 scenario. The spatial distribution of extreme precipitation indices shows intensification over the eastern part of South Asia compared to the western part. The probability density function of extreme precipitation indices suggests a frequent (intense) occurrence of precipitation extremes in the FF period under the SSP5-8.5 scenario, with values up to 35.00 d for RR1mm and 25.00–35.00 d for CWD. The potential impacts of heavy precipitation can pose serious challenges to the study area regarding flooding, soil erosion, water resource management, food security, and agriculture development.

Keywords: precipitation extremes; extreme precipitation indices; climate change; Coupled Model Intercomparison Project 6 (CMIP6); Global Climate Model (GCM); South Asia

Citation: Adnan ABBAS, Asher S BHATTI, Safi ULLAH, Waheed ULLAH, Muhammad WASEEM, ZHAO Chengyi, DOU Xin, Gohar ALI. 2023. Projection of precipitation extremes over South Asia from CMIP6 GCMs. Journal of Arid Land, 15(3): 274–296. https://doi.org/10.1007/s40333-023-0050-3

*Corresponding author: ZHAO Chengyi (E-mail: zhaocy@nuist.edu.cn)
The first and second authors contributed equally to this work.
Received 2022-05-10; revised 2022-10-09; accepted 2022-10-13

1 Introduction

Global warming has resulted in climate variability and changes that have increased the uncertainty of extreme hydrological events worldwide (Christensen and Christensen, 2004; Shiu et al., 2012; Papalexiou and Montanari, 2019; Shen et al., 2022; Yu et al., 2023). According to the Sixth Assessment Report of the Intergovernmental Panel on Climate Change (IPCC-AR6), climate change has altered the frequency and intensity of precipitation extremes with severe consequences (IPCC, 2021). The recent State of the Global Climate 2021 report of the World Meteorological Organization (WMO) stated that precipitation extremes had caused many causalities and tremendous socioeconomic losses over the past 50 years (1970–2019) (WMO, 2021). The accounted death toll was over 0.059×10^6 from the flooding and 0.650×10^6 from the drought during 1970–2019 (WMO, 2021) Moreover, literature has witnessed the occurrence of such extreme precipitation events globally, for instance, the 2010 floods in Pakistan, the 2011 floods in the United States of America (USA) (Hussain et al., 2018; Khan et al., 2022), the 2015 floods in India and Nepal, the 2009 and 2011 flash flooding in Saudi Arabia, and coastal flooding in Venice of the Italy (2019), Karachi of Pakistan (2020), and Mumbai of India (2021) (Almazroui et al., 2016, 2018; Phillips, 2020; Herring et al., 2021).

Global warming has triggered the intensification of such extreme precipitation events in tropical regions by changing the water vapor contents of the atmosphere, moisture supply, and circulation pattern (Ullah et al., 2020; Shen et al., 2022), which damages the ecosystem, further amplifying water and food security challenges (Allen and Ingram, 2002; Held and Soden, 2006; Vecchi et al., 2006; Hulme, 2016; Marotzke et al., 2017; Sillmann et al., 2017; Nikulin et al., 2018; Chen and Sun, 2019). It is, therefore, crucial to assess and understand the changes in future precipitation extremes so that the climate-induced water security challenges can be better addressed (Nooni et al., 2021; Abbas et al., 2022). Many studies have been conducted across the globe to assess the variations in future precipitation intensity by using Coupled Model Intercomparison Project (CMIP) Global Climate Models (GCMs). Watterson and Rafter (2017) projected the monthly and daily precipitation of Australia using the simulations of 33 ensembles of Coupled Model Intercomparison Project Phase 5 (CMIP5) GCMs under the RCP8.5 (where RCP is the Representative Concentration Pathway) scenario and compared the results with six simulations from the downscaled Conformal Cubic Atmospheric Model (CCAM). These models reveal the increasing tendency of precipitation in the future. Li et al. (2016) projected a 20% increase in total precipitation over western China towards the end of the 21st century. Thibeault and Seth (2014) employed 23 CMIP5 GCMs to evaluate extreme precipitation indices for the northeastern USA and Canada. Their results anticipated an increase in total annual precipitation, which was strongly associated with the increase in extreme wet winters. In another study, Almazroui et al. (2021) assessed that average precipitation in most parts of the USA is expected to increase by 10%–30%, showing more variations.

The current study is carried out over South Asia that is characterized by complicated atmospheric dynamics and climatic processes. The climate of South Asia is marked by high temperature and humidity, with substantial seasonal variations (Ullah et al., 2019a), including the monsoon season with considerable rainfall. South Asia, home to one-fifth of the total world's population, is one of the most sensitive regions in the world to climate change since its water resources and agriculture are highly exposed to climate change extremes (Bandara and Cai, 2014). Most of the river deltas in South Asia are heavily populated and are significantly dependent on agriculture for livelihood. The changing climate is putting pressure on water resources, which can lead to a high risk of water scarcity in this region (Zhai et al., 2020; Syed et al., 2022). The fast melting of glaciers, increasing unpredictability of monsoon precipitation, and the increased frequency of precipitation extremes render the people of South Asia more vulnerable to climate change (Immerzeel et al., 2015). Furthermore, climate change is expected to have an impact on food security by the middle of the 21st century, with South Asia having the highest number of food-insecure regions (IPCC, 2014).

South Asia is considered one of the global hotspot regions in terms of climate change vulnerability, and the risk of extreme precipitation events is likely to increase in South Asia in the future, which could have negative impacts on water and agriculture sectors (Turner and Annamalai, 2012; Ullah et al., 2021a). The mean monsoon precipitation is projected to increase by 8% in South Asia (Kripalani et al., 2007). Since the majority of the population in South Asia develops their economies through agriculture, thus, their living standards could be adversely affected by precipitation extremes (Frona et al., 2021). In recent decades, the frequency and intensity of precipitation extremes have considerably increased, which will continue in the future with more dramatic impacts across the globe, including South Asia (Tabari, 2020). Therefore, it is critical to assess the future changes in precipitation extremes using the latest GCMs.

The present study employs Coupled Model Intercomparison Project Phase 6 (CMIP6) GCMs to analyze the spatiotemporal variability of projected precipitation extremes over South Asia. The spatiotemporal variations in precipitation and its extremes may cause the shift in drought and flooding patterns over the region; it is, therefore, important to understand this variability so that associated socioeconomic impacts can be lessened. The results of this study have significant implications for government policymakers and water and agriculture sectors as they work to implement high-priority mitigation and adaptation measures in the coming decades.

2 Study area

South Asia (Fig. 1) is located between 5°–40°N latitudes and 60°–100°E longitudes, with a total landmass of approximately 5.134×10^6 km^2 (Ramachandran and Kedia, 2013; Tariq and Ali, 2017; Ullah et al., 2022a). The region is characterized by complex topography, as it includes the world's highest mountain ranges (i.e., the area with the towering Himalayas) in the north, the Indian Ocean in the south, and plains and deserts in the central part (Ren et al., 2017; Sun et al., 2017; Ullah et al., 2022b). The present study divides South Asia into three subregions according to its geography: northern subtropical monsoon subregion (R1), eastern tropical monsoon subregion (R1), and westerly subregion (R3), while the Indian Ocean is the southern periphery.

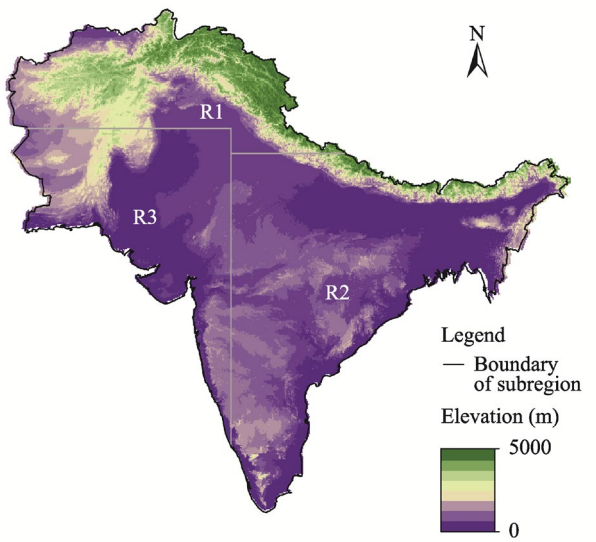

Fig. 1 Spatial distribution of elevation in South Asia and its three subregions (R1, R2, and R3). R1, northern subtropical monsoon subregion; R2, eastern tropical monsoon subregion; R3, westerly subregion.

The climate in South Asia varies from arctic temperature in the high mountainous areas to temperate conditions in the northern areas, and to tropical conditions in the central and southern areas (Tariq and Ali, 2017; Ullah et al., 2018). The diverse topography and geographical location of South Asia significantly affect the seasonal and annual variations in precipitation and

temperature, which ultimately influence the overall climate of this region (Sun et al., 2017; Ullah et al., 2019b). The hydrological cycle in South Asia is governed by the monsoon circulation system and western disturbances (Li et al., 2017; Hunt et al., 2018; Chen et al., 2019; Khan et al., 2020). These weather systems influence the intensity of regional precipitation and temperature both directly and indirectly. The western disturbances, which are low-pressure systems, originate from the Mediterranean Sea and contribute to the hydrological cycle of Afghanistan, Pakistan, India, and neighboring countries during the winter season (Filippi et al., 2014; Dimri et al., 2015; Ahmed et al., 2018; Ullah et al., 2021b). Furthermore, these systems cause less precipitation compared to the monsoon system, but their occurrence is closely associated with the food security of this region, particularly in rain-fed areas of South Asia (Yadav and Lal, 2018; Ahmed et al., 2019). Summer monsoons, the second most important precipitation system, dominate the region from June to September and account for 65% of the water cycle's precipitation (Medina et al., 2010; Joshi and Kar, 2018). If any of these two (monsoon and western disturbance) weather systems become fail in producing the required precipitation amount, then it affects the regional water supply and causes droughts, ultimately reducing regional crop yield (Azad et al., 2013; Rasmussen et al., 2015; Latif et al., 2017; Gupta and Jain, 2018; Wu et al., 2019).

3 Data and methods

3.1 Data collection

The study used daily precipitation data for the two time periods (i.e., near future (NF; 2021–2060) and far future (FF; 2061–2100)), which were obtained from the CMIP6 data archives (https://esgf-node.llnl.gov/search/cmip6/) for the 21st century. The details of the selected models are given in Table 1.

Table 1 Details of the selected Coupled Model Intercomparison Project Phase 6 (CMIP6) Global Climate Models (GCMs)

No.	Model Name	Country	Resolution
1	BCC-CSM2-MR	China	1.1°×1.1°
2	CanESM5	Canada	2.8°×2.8°
3	CESM2-WACCM	United States of America	1.3°×0.9°
4	CNRM-CM6-1	France	1.4°×1.4°
5	CNRM-ESM2-1	France	1.4°×1.4°
6	IPSL-CM6A-LR	France	2.5°×1.3°
7	MIROC6	Japan	1.4°×1.4°
8	MPI-ESM1-2-HR	Germany	0.9°×0.9°
9	MRI-ESM2-0	Japan	1.1°×1.1°
10	NESM3	China	1.9°×1.9°

The future changes in precipitation extremes were estimated in two time periods (i.e., NF and FF) of the 21st century under two Shared Socioeconomic Pathway (SSP) scenarios (i.e., SSP2-4.5 and SSP5-8.5), which are the new scenarios developed to project socioeconomic global changes up to 2100 and are considered as key aspects in climate risk assessments with different climate policies (Andrijevic et al., 2021). SSPs play a vital role in climate adaptation and policy work for two main reasons. First, SSPs describe possible socioeconomic conditions (including land-use changes) and other anthropogenic climate drivers; and second, SSPs describe socioeconomic characteristics that influence greenhouse gas emissions, indicating the different levels of warming associated with socioeconomic pathways (Riahi, 2016). SSP-based scenarios were used in the recent set of climate model experiments, known as CMIP6. Results from this project provide the assessments of past and future climate change in the IPCC-AR6. The details of results for SSP scenarios are listed in the IPCC-AR6 (IPCC, 2021; Lehtonen et al., 2021). As the selected CMIP6 GCMs have different resolutions, we used a bilinear interpolation technique to interpolate the

selected models into a common grid resolution of 0.5°×0.5° (Ullah et al., 2022a), which facilitates the comparison between simulated outputs of various models. Subsequently, the graphical files for the South Asian regions were used to mask the simulated precipitation data for further analysis.

3.2 Precipitation indices

The present study used eight extreme precipitation indices from the list of the Expert Team on Climate Change Detection and Indices (ETCCDI) of the WMO (Zhang et al., 2011; Ongoma et al., 2018). Table 2 explains the description of the selected indices. These indices were appropriate to assess and examine the variations in precipitation extremes over South Asia.

Table 2 Description of the selected extreme precipitation indices used in this study

Index	Abbreviation	Definition	Unit
Wet days	RR1mm	Annual count of days when precipitation ≥1.00 mm	d
Heavy precipitation days	RR10mm	Annual count of days when precipitation ≥10.00 mm	d
Very heavy precipitation days	RR20mm	Annual count of days when precipitation ≥20.00 mm	d
Severe precipitation days	RR50mm	Annual count of days when precipitation ≥50.00 mm	d
Consecutive wet days	CWD	Annual maximum number of consecutive days with precipitation >1.00 mm	d
Consecutive dry days	CDD	Annual maximum number of consecutive days with precipitation <1.00 mm	d
Max 5-day precipitation amount	RX5day	Annual maximum 5-day consecutive precipitation	mm
Simple daily intensity index	SDII	Mean precipitation amount on wet days	mm/d

Note: These extreme precipitation indices are recommended by the Expert Team on Climate Change Detection and Indices (ETCCDI).

3.3 Statistical analysis

This study employed different statistical techniques, such as Sen's slope estimator (Sen, 1968), modified Mann-Kendall test (Hamed and Rao, 1998), Student's *t*-test (Ullah et al., 2019b), and probability density function to assess the spatiotemporal variations in future precipitation extremes over South Asia. The individual models and their ensemble mean (known as multi-model ensemble mean (MMEM)) were used to project the spatiotemporal changes in future precipitation extremes over the study area. The non-parametric Sen's slope estimator test was applied to estimate the magnitude of future changes, while the modified Mann-Kendall test was used to determine the significant changes at the 0.05 significance level. The student's *t*-test was used to detect the significant linear trends in the extreme precipitation indices for the future period. Many researchers around the globe have widely used these techniques in their studies on climate and hydrology (Bhatti et al., 2020; Ullah et al., 2020; Abbas et al., 2022).

3.3.1 Sen's slope estimator

The present study used Sen's slope estimator to examine the magnitude of future variations in extreme precipitation indices, and the amplitude was assumed to be linear. The Sen's slope (S_{ij}) can be calculated as to estimate each individual slope:

$$\text{Sen's slope}\,(S_{ij}) = \text{median}\left(\frac{x_j - x_i}{j - i}\right)\ (i < j)\,, \tag{1}$$

where x_i and x_j are the sequential data for the i^{th} and j^{th} terms (where j is greater than i). The Sen's slope estimator was applied with the boundary (lower and upper limits) of the confidence interval (1–α), where the significance level (α) was stated as default (α=0.05). The test can be used for time series data x_i if i=1, 2, 3,…, n–1, and x_j if j=k+1, k+2, k+3, …, n. Suppose we have n values of x_j in the time series, then, N=n(n–1)/2, and the median of N values of S is known as Sen's slope. The Sen's slope is described as follows:

$$S = 1/2\left[S_{(N/2)} + S_{\{(N+1)/2\}}\right] \quad \text{if } N \text{ is even}, \tag{2}$$

$$S = S_{\{(N+1)/2\}} \quad \text{if } N \text{ is odd}, \tag{3}$$

where N is the number of pairs of time series elements (x_i, x_j). Positive Sen's slope shows an upward trend while negative Sen's slope reveals a downward trend. Consequently, it is possible to calculate a two-sided confidence interval for the slope of the confidence interval (1–α).

3.3.2 Modified Mann-Kendall test

The modified Mann-Kendall test was used to demonstrate the projected changes in precipitation extremes at the 0.05 significance level. The standardized statistic 'Z' is given after variance correction, to remove the influence of serial correlation on this trend test (Hamed and Ramachandra Rao, 1998; Blain, 2013; Ullah et al., 2020). The variance of the trend statistic S ($Var(S)$; also known as the Mann-Kendall statistic) of the autocorrelation series is stated herein for the assessment of statistic Z using Equations 4 and 5 (Alashan, 2020; Bhatti et al., 2020), in which n refers to the data points number.

$$Var(S) = n(n-1)(2n+5)/18, \tag{4}$$

$$Z = \begin{cases} \dfrac{S-1}{\sqrt{Var(S)}}, & \text{if } S > 0 \\ 0, & \text{if } S = 0 \\ \dfrac{S+1}{\sqrt{Var(S)}}, & \text{if } S < 0 \end{cases}. \tag{5}$$

3.3.3 Student's *t*-test

The student's t-test is a popular technique for determining the significance of time series. This test was employed to find the significant linear trend in projected extreme precipitation indices using the signal-to-noise ratio (t-value). For climate simulation study, signal refers to climate change caused by external forcing, which is calculated as the difference between the averaging of simulated precipitation and hypothesized values. Noise indicates the internal variability in climatic simulation, which is calculated from the variability information in the time series (Iqbal et al., 2016; Wen et al., 2017; Abbas et al., 2018; Rahman et al., 2018; Jiang et al., 2019; Shen et al., 2022). The mathematical formula for the student's t-test is given below:

$$t = \frac{m-\mu}{s/\sqrt{n}}, \tag{6}$$

where t is the student's t-test; m is the mean value; μ is the hypothesized value; s is the standard deviation; and n is the sample size (i.e., the data length of the time series).

3.3.4 Probability density function

The probability density function was used to observe the relative density of precipitation extremes in the NF and FF periods under the SSP2-4.5 and SSP5-8.5 scenarios. The probability density function is a non-parametric method using kernel density estimation on a random sample. The kernel density estimation usually describes the distribution pattern, allowing for the input to shape the distribution pattern and moments of the distribution. The general formula of the kernel density estimator is shown as follows:

$$\hat{f}_h(x) = \frac{1}{n}\sum_{i=1}^{n} K_h(x-x_i) = \frac{1}{nh}\sum_{i=1}^{n} K\left(\frac{x-x_i}{h}\right), \tag{7}$$

where x (x_1, x_2, …, x_i) is an independent parameter; $\hat{f}$ is the unknown density at any given point of x; K is the kernel density estimation (a non-negative function); and h is the bandwidth with a smoothing parameter (h>0).

In addition, box plots were plotted to assess the absolute variations in extreme precipitation indices in the NF and FF periods under the SSP2-4.5 and SSP5-8.5 scenarios over South Asia.

The box-plot method is an ideal way to observe the skewness and trend in future climatic indices, which can help us to find the comparison in multiple datasets at the same time (Ullah et al., 2021b).

4 Results

4.1 Temporal changes in extreme precipitation indices

The selected individual CMIP6 GCM and its MMEM were employed to project the long-term temporal variations in future precipitation extremes over the study area. Figures 2 and 3 illustrate long-term area-averaged temporal trends of extreme precipitation indices in the NF and

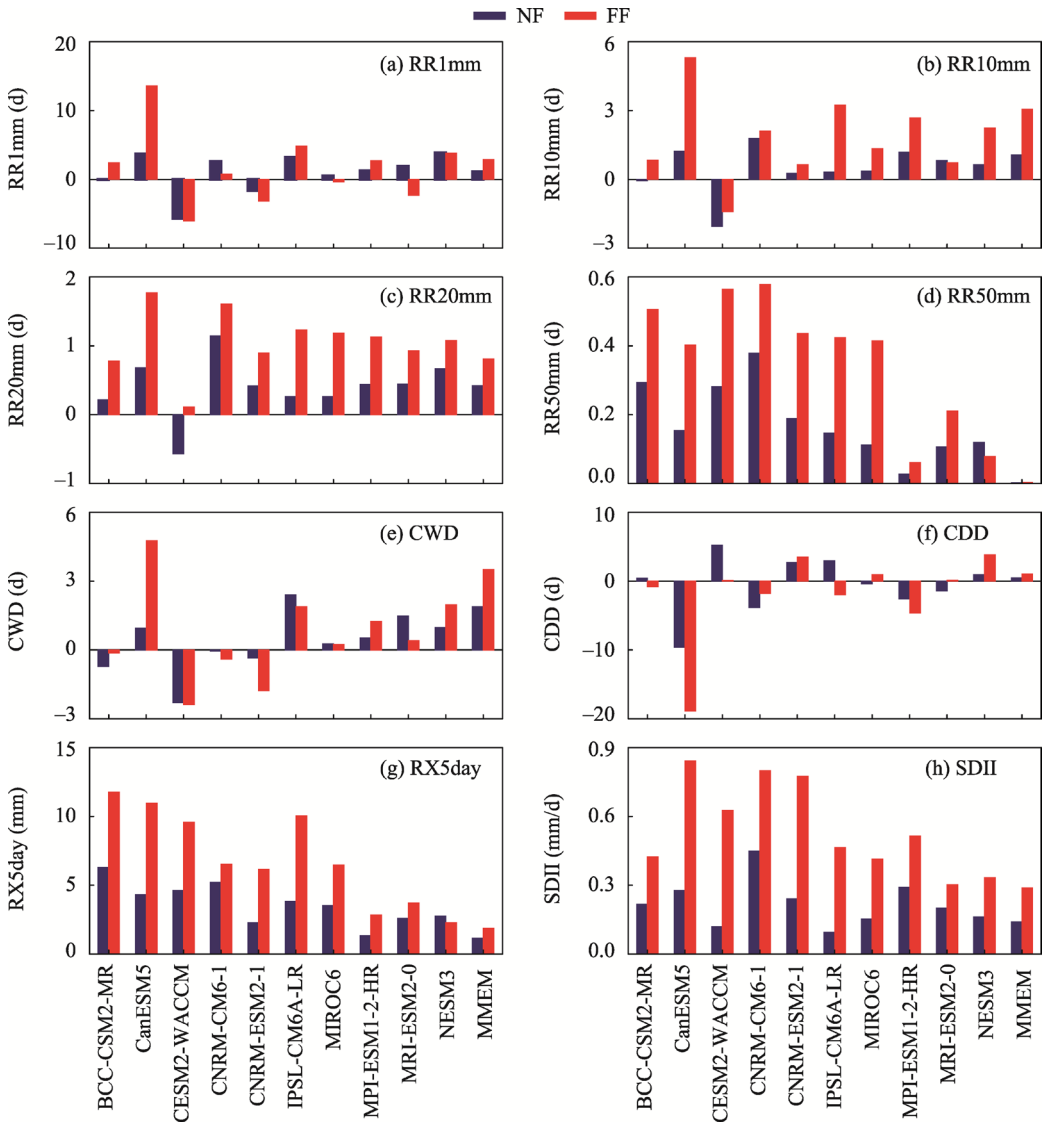

Fig. 2 Long-term temporal changes in extreme precipitation indices of CMIP6 GCMs and MMEM in the NF and FF periods under the SSP2-4.5 scenario. CMIP6, Coupled Model Intercomparison Project Phase 6; GCMs, Global Climate Models; MMEM, multi-model ensemble mean; NF, near future (2021–2060); FF, far future (2061–2100); SSP, Shared Socioeconomic Pathway. (a), RR1mm (wet days); (b), RR10mm (heavy precipitation days); (c), RR20mm (very heavy precipitation days); (d), RR50mm (severe precipitation days); (e), CWD (consecutive wet days); (f), CDD (consecutive dry days); (g), RX5day (max 5-day precipitation amount); (h), SDII (simple daily intensity index). The negative values indicate a decreasing trend, while the positive values indicate an increasing trend.

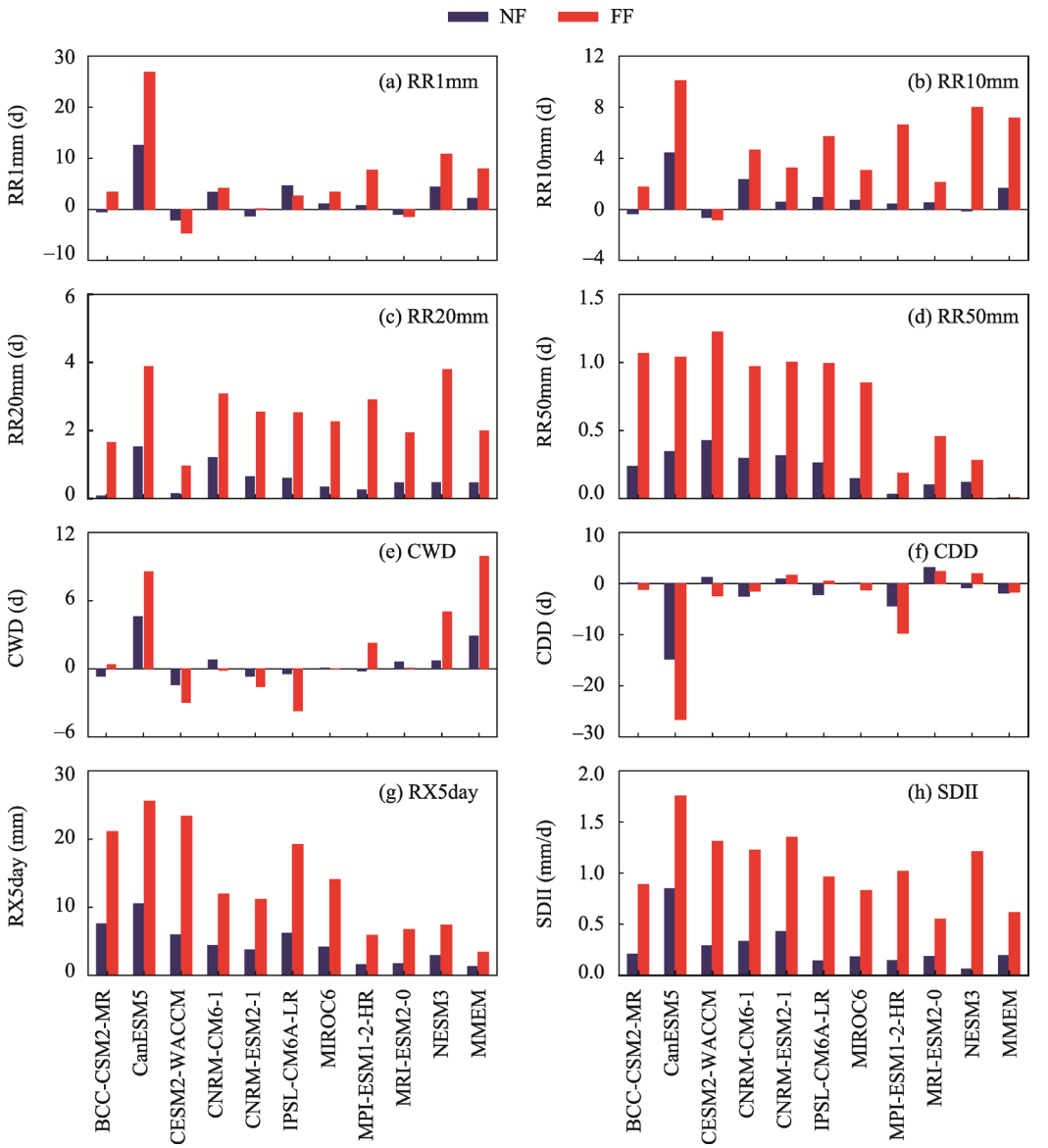

Fig. 3 Long-term temporal changes in extreme precipitation indices of CMIP6 GCMs and MMEM in the NF and FF periods under the SSP5-8.5 scenario. (a), RR1mm; (b), RR10mm; (c), RR20mm; (d), RR50mm; (e), CWD; (f), CDD; (g), RX5day; (h), SDII. The negative values indicate a decreasing trend, while the positive values indicate an increasing trend.

FF periods under the SSP2-4.5 and SSP5-8.5 scenarios, respectively. From the results it can be seen that most of the indices indicate an increasing trend of precipitation extremes in the FF period under the SSP5-8.5 scenario. This implies that the study area will experience frequent and intense precipitation extremes by the end of the 21st century under the high emission scenario.

The results of each model show a clear discrepancy between their lowest and highest values, which could be attributed to the presence of uncertainty in their projections (Chen et al., 2020). Additionally, the uncertainty of circulation changes caused by the sea surface temperature may be linked to the uncertainty of precipitation variations over the study area (Endo and Kitoh, 2014; Chen and Zhou, 2015; Zhou et al., 2018).

The results (including the MMEM) under the SSP2-4.5 scenario (Fig. 2a) show that almost all selected CMIP6 GCMs project fewer occurrence of wet days (RR1mm) in both periods (NF and FF) with no significant difference, while only one model, i.e., CanESM5, reveals a slightly

difference in the occurrence of RR1mm between the NF and FF periods (considerable difference value up to 13.00 d). The analysis suggests that almost all models reveal significant increases in the occurrence of heavy precipitation days (RR10mm), very heavy precipitation days (RR20mm), and severe precipitation days (RR50mm) in the FF period, with values increasing up to 6.00, 2.00, and 1.00 d, respectively (Fig. 2b–d). Similarly, the results for consecutive wet days (CWD) indicate the maximum occurrence in the FF period, and the number of RR1mm ranges between 1.00 and 5.00 d from the NF period to the FF period (Fig. 2e). However, no significant difference is observed in the occurrence of consecutive dry days (CDD) during either period (see Fig. 2f). It is observed from the results of max 5-day precipitation amount (RX5day) and simple daily intensity index (SDII) that there is a simultaneous increase in the occurrence of both indices towards the end of the century (Fig. 2g and h). The overall results from this study reveal that all models report an increase in the frequency and intensity of disasters such as flooding, landslides, and loss of crops, which can threaten human lives due to precipitation extremes under the SSP2-4.5 scenario over this region.

Figure 3 describes the results for extreme precipitation indices projected under the SSP5-8.5 scenario. Similar to the SSP2-4.5 scenario, the results under the SSP5-8.5 scenario reveal an increase in the tendency of extreme precipitation indices in the FF period. It is evident from Figure 3a that the MMEM shows low occurrence of RR1mm in the NF and FF periods, with a projected increase of up to 9.00 d in the late century (FF period) under the SSP5-8.5 scenario. Meanwhile, the MMEMs of RR10mm and RR20mm reveal significant increases of 7.90 and 1.90 d in the FF period (Fig. 3b and c), respectively. In Figure 3d, RR50mm is higher in the FF period, and noteworthy change is observed, ranging from 0.20 to 1.30 d; however, its MMEM reveals no evident occurrence in either time period. While performing further analyses on duration indices (i.e., CWD and CDD), continuous variations are found. The result of CWD (Fig. 3e) indicates a considerable increase (up to 10.00 d) in the MMEM in the FF period under the SSP5-8.5 scenario, which reveals intensification in the duration of CWD during 2061–2100. The MMEM of CDD (Fig. 3f) describes a slight wetting pattern, ranging from 0.00 to –1.00 d (negative trend) in the FF period, which depicts a decreasing trend by the end of the 21st century. The assessment of the RX5day index (Fig. 3g) reveals no considerable change in the amount of precipitation in the FF period, and the projected increase is up to 4.00 d under the SSP5-8.5 scenario. Similarly, a remarkable increase is expected to appear in the occurrence of SDII in the late century, and the intensity of MMEM increases with the magnitude >0.60 mm/d under the high emission scenario (SSP5-8.5) (Fig. 3h).

4.2 Spatial distribution of extreme precipitation indices

Figures 4–7 present the spatial distribution of projected extreme precipitation indices in South Asia in the NF and FF periods under two SSP scenarios. The black dots describe the trend inferred from the modified Mann-Kendall test as statistically significant at the 0.05 significance level over the respective subregions by applying the student's *t*-test. Similar to the temporal distribution, the spatial patterns of extreme precipitation indices over South Asia were also analyzed in the NF and FF periods under both scenarios (SSP2-4.5 and SSP5-8.5). Under the SSP2-4.5 scenario, the spatial distribution of projected extreme precipitation indices describes the spatial variations of RR1mm from the western to the eastern part of South Asia in the NF and FF periods (Fig. 4a and b). However, a significant increasing trend of RR1mm is noticed in most parts of South Asia under the SSP2-4.5 scenario, with the highest value up to 42.00 d in the central area. Noticeably, a distinct change in the spatial extent of RR10mm is observed under the SSP2-4.5 scenario in both future periods (Fig. 4c and d). In the NF period, most parts of South Asia (including eastern India, Bangladesh, and Bhutan) exhibit a significant increasing trend in RR10mm (up to 30.00 d), whereas this trend decreases in the northwestern parts of Afghanistan and Pakistan in the FF period. The spatial distribution of RR20mm shows a moderate change in both the NF and FF periods (Fig. 4e and f).

Results for RR50mm under the SSP2-4.5 scenario (Fig. 4g and h) reveal no remarkable change

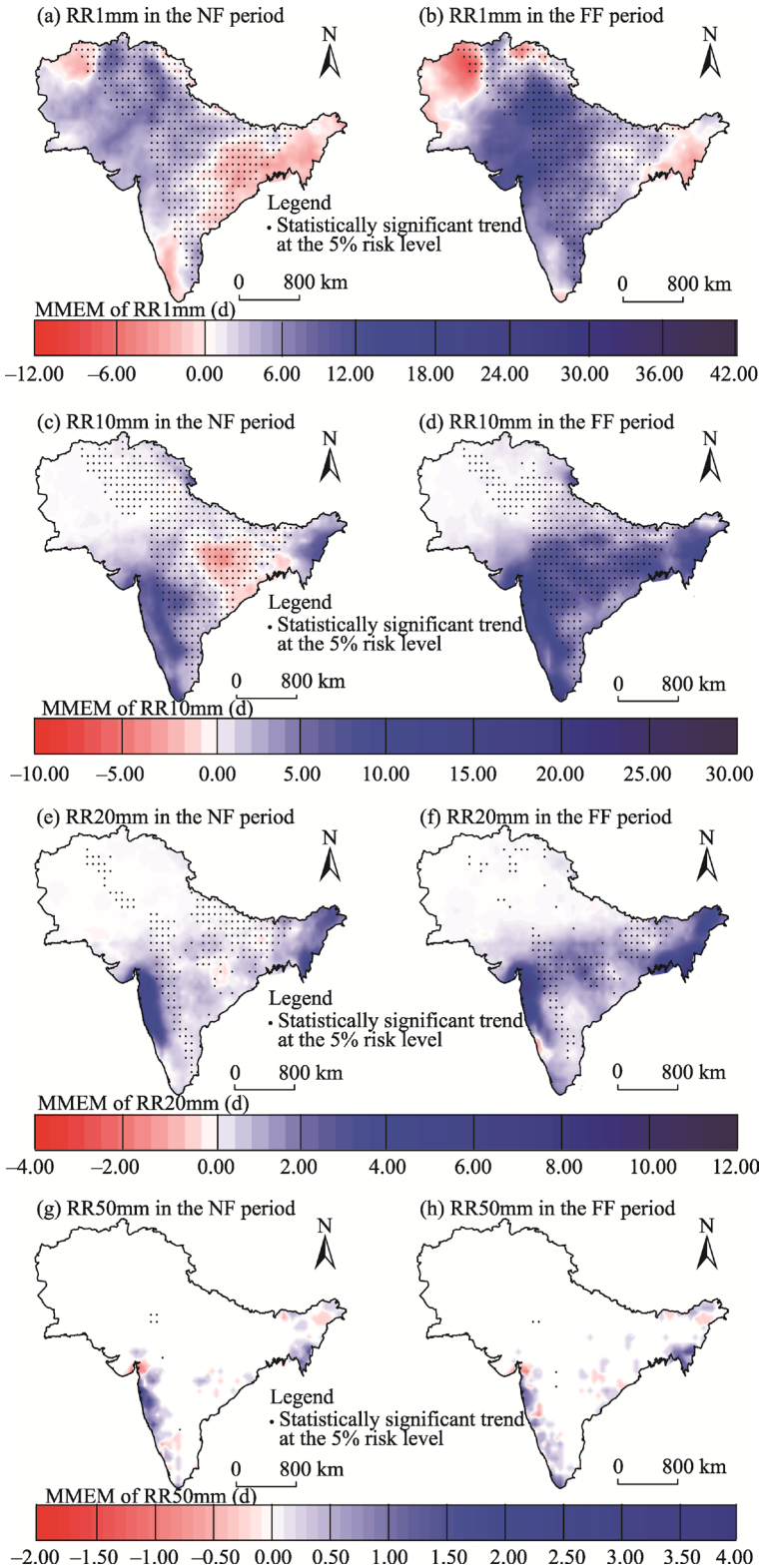

Fig. 4 Spatial distribution of changes in the MMEMs of RR1mm (a and b), RR10mm (c and d), RR20mm (e and f), and RR50mm (g and h) in the NF and FF periods under the SSP2-4.5 scenario. The black dot indicates that the trend is statistically significant at the 5% risk level at each grid point. The negative values indicate a decreasing trend, while the positive values indicate an increasing trend.

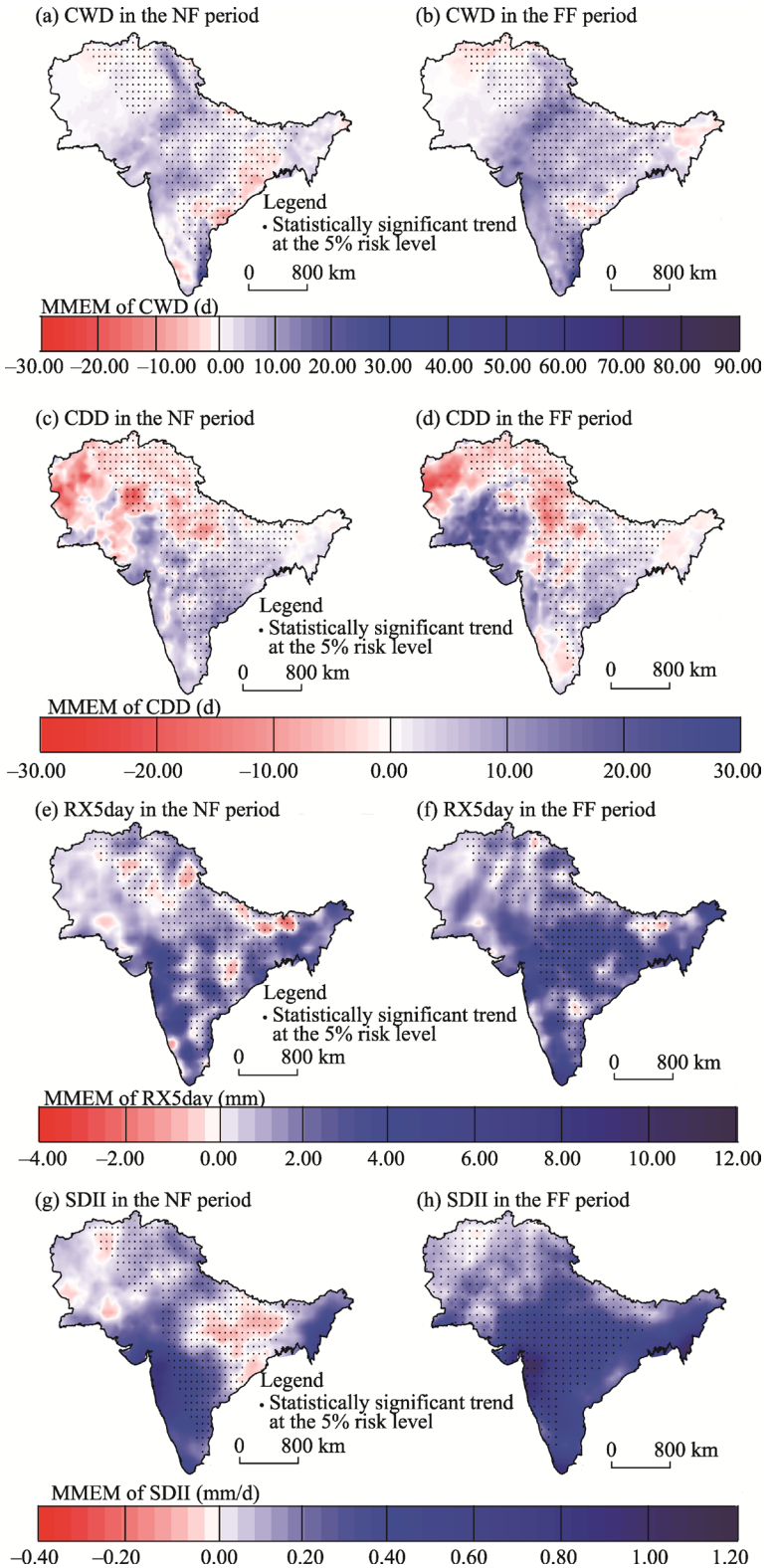

Fig. 5 Spatial distribution of changes in the MMEMs of CWD (a and b), CDD (c and d), RX5day (e and f), and SDII (g and h) in the NF and FF periods under the SSP2-4.5 scenario. The black dot indicates that the trend is statistically significant at the 5% risk level at each grid point. The negative values indicate a decreasing trend, while the positive values indicate an increasing trend.

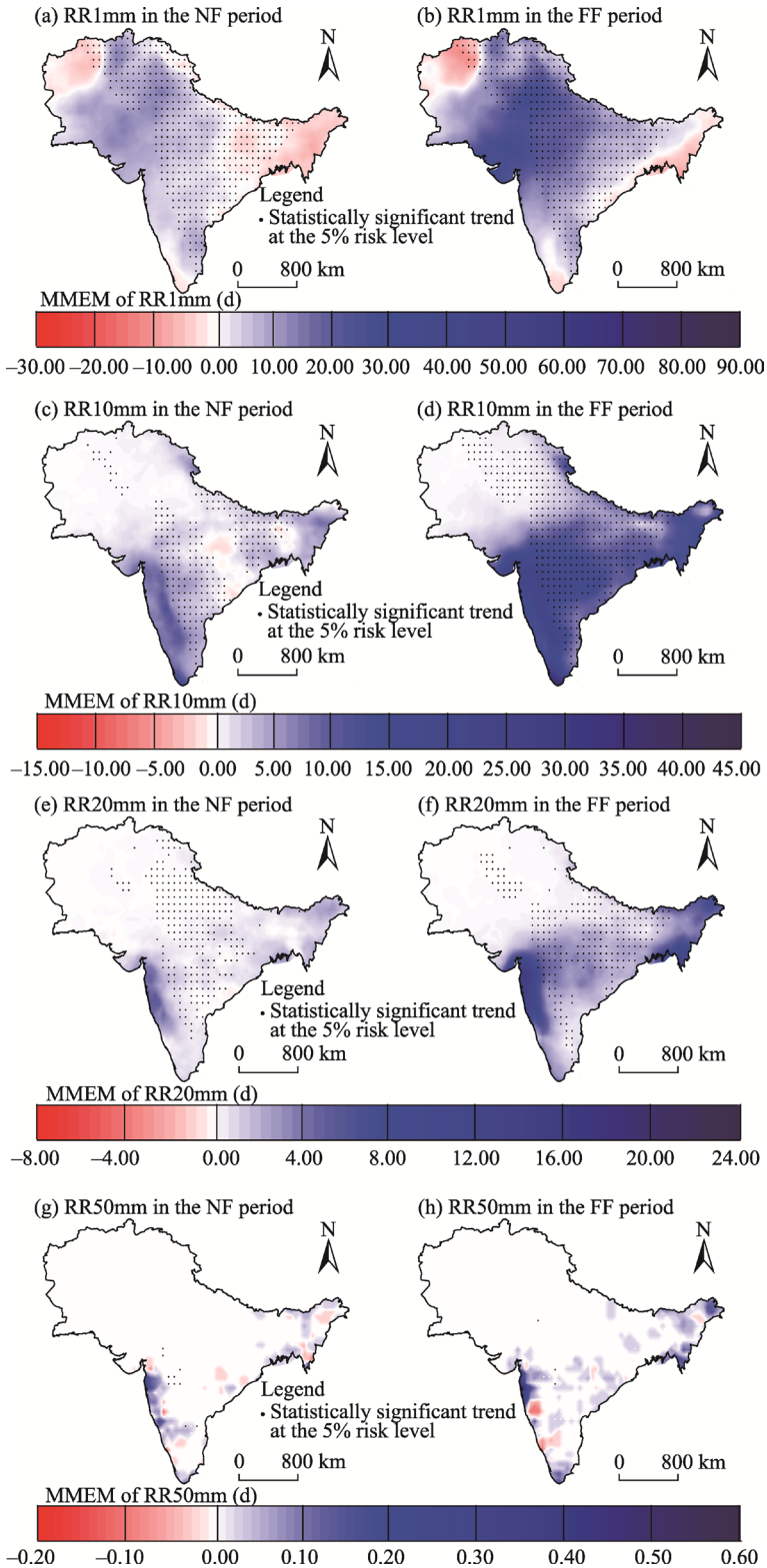

Fig. 6 Spatial distribution of changes in the MMEMs of RR1mm (a and b), RR10mm (c and d), RR20mm (e and f), and RR50mm (g and h) in the NF and FF periods under the SSP5-8.5 scenario. The black dot indicates that the trend is statistically significant at the 0.05 significance level at each grid point. The negative values indicate a decreasing trend, while the positive values indicate an increasing trend.

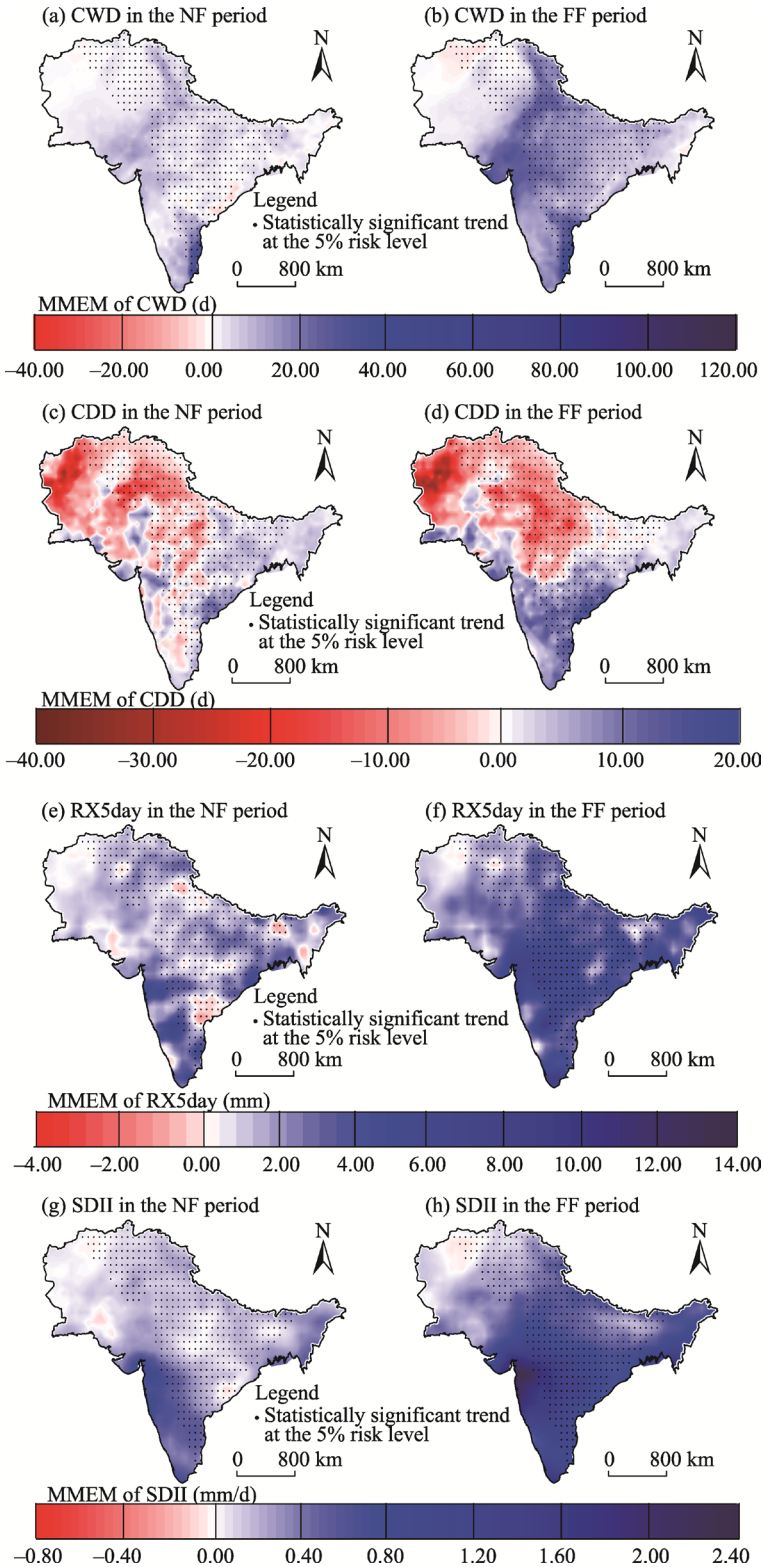

Fig. 7 Spatial distribution of changes in the MMEMs of CWD (a and b), CDD (c and d), RX5day (e and f), and SDII (g and h) in the NF and FF periods under the SSP5-8.5 scenario. The black dot indicates that the trend is statistically significant at the 0.05 significance level at each grid point. The negative values indicate a decreasing trend, while the positive values indicate an increasing trend.

in both time periods and the spatial extent of RR50mm is limited to a small portion in southern India and southeastern Bangladesh. In other words, no considerable occurrence of RR50mm is projected under the SSP2-4.5 scenario. However, it is found that the spatial extent of precipitation decreases from RR1mm to RR50mm over South Asia and the amount of precipitation also reduces from the northwestern to the southeastern part of South Asia. The duration indices (CWD and CDD) and RX5day show no considerable change in the spatial extent of the significant trend. The occurrence of CWD under the SSP2-4.5 scenario (Fig. 5a and b) increases to some extent (10.00–40.00 d) from the central to the eastern part of South Asia and the occurrence of CDD under the SSP2-4.5 scenario (Fig. 5c and d) increases (up to 30.00 d) in the southern part of Pakistan during 2061–2100 (FF period). In the FF period, RX5day under the SSP2-4.5 scenario is projected to appear with high intensity in the eastern part of South Asia, but its scatter impacts are also observed in some western regions, with the intensity being up to 3.00–4.00 mm (Fig. 5e and f). The spatial distribution of SDII under the SSP2-4.5 scenario exhibits an increasing trend throughout the study area (except some eastern regions), and the increasing trend is up to 1.20 mm/d in the central part and most of the eastern part; however, as with other indices, the western part is less influenced by SDII in terms of intensity and occurrence (Fig. 5g and h).

Figures 6 and 7 show the spatial distribution of projected precipitation extremes under the SSP5-8.5 scenario in the NF and FF periods. The projected change in the regional distribution of RR1mm under the SSP5-8.5 scenario (Fig. 6a and b) is comparable to that under the SSP2-4.5 scenario (Fig. 4a and b), but there is a steady increase in the intensity of RR1mm (90.00 d), which reflects that future precipitation can pose severe challenges in terms of flooding, soil erosion, water resources management, food security, and agriculture development. In the case of RR10mm under the SSP5-8.5 scenario (Fig. 6c and d), a sharp and considerable increasing trend is noted across the upper parts of South Asia in the FF period. On the other hand, the eastern and southeastern parts are anticipated to get up to 45.00 mm of precipitation. For RR20mm under the SSP5-8.5 scenario (Fig. 6e and f), its intensity and spatial extent will increase in the FF period as compared to the NF period, with the intensity being up to 24.00 d. Under the SSP5-8.5 scenario, no significant change is observed in the spatial extent of RR50mm (Fig. 6g and h) in both periods. For CWD (Fig. 7a and b) and CDD (Fig. 7c and d), their spatial distribution does not mark any considerable changes in the significant trend in both periods, but CWD increases and CDD decreases in the late century under the SSP5-8.5 scenario. Moreover, the projected changes in RX5day (Fig. 7e and f) and SDII (Fig. 7g and h) under the SSP5-8.5 scenario depict an increase in the spatial extent from the central to the eastern part of the study area in the FF period.

Overall, it has been assessed from the results that both scenarios are expected to produce extreme precipitation towards the end of the century, but its intensity will become more obvious under the SSP5-8.5 scenario than under the SSP2-4.5 scenario. The significant observation at each grid point shows that the eastern part of South Asia is more likely to experience severe precipitation than the western part in ascending order to obtain the annual precipitation sequence for every year from the NF period to the FF period, which may cause extreme hydrological events (i.e., flood and drought) at the same time over the study area.. Therefore, this study is the need for the projection of extreme precipitation indices over South Asia for a better understanding and risk assessment of the possible future changes in precipitation extremes.

4.3 Probability distribution of precipitation extremes

Figure 8 shows the relative probability distribution of extreme precipitation events in the NF and FF periods under the SSP2-4.5 and SSP5-8.5 scenarios over South Asia. The overall distribution plots reveal that compared with the NF period, the distribution curves in the FF period skew towards the right and turn flattered to some extent under the selected scenarios.

In South Asia, the distribution of RR1mm in the FF period under the SSP2-4.5 and SSP5-8.5 scenarios shows a shift to the right side, describing the increase in RR1mm as compared to the NF period (Fig. 8a). The RR1mm in the NF is relatively normally distributed and does not show a significant change in the magnitude but slightly differ in their frequency. A corresponding

distribution pattern for RR10mm and RR20mm in the FF period under a high emission scenario (SSP5-8.5) is observed (Fig. 8b and c); however, there is a distinguished shift in curves to the right side and the curves become somehow flattened for RR20mm, showing an increase in the intensity of precipitation but a decrease in the frequency of precipitation, which may lead to the intensification of the water cycle in the future (Hanf et al., 2017). Under the SSP5-8.5 scenario, the RR50mm curves shift to the right in the FF period, and the simulated maximum precipitation value reaches up to 0.04 mm (Fig. 8d). The distribution patterns of RR50mm curves are different from those of other extreme precipitation indices, due to the appearance of some small peaks on

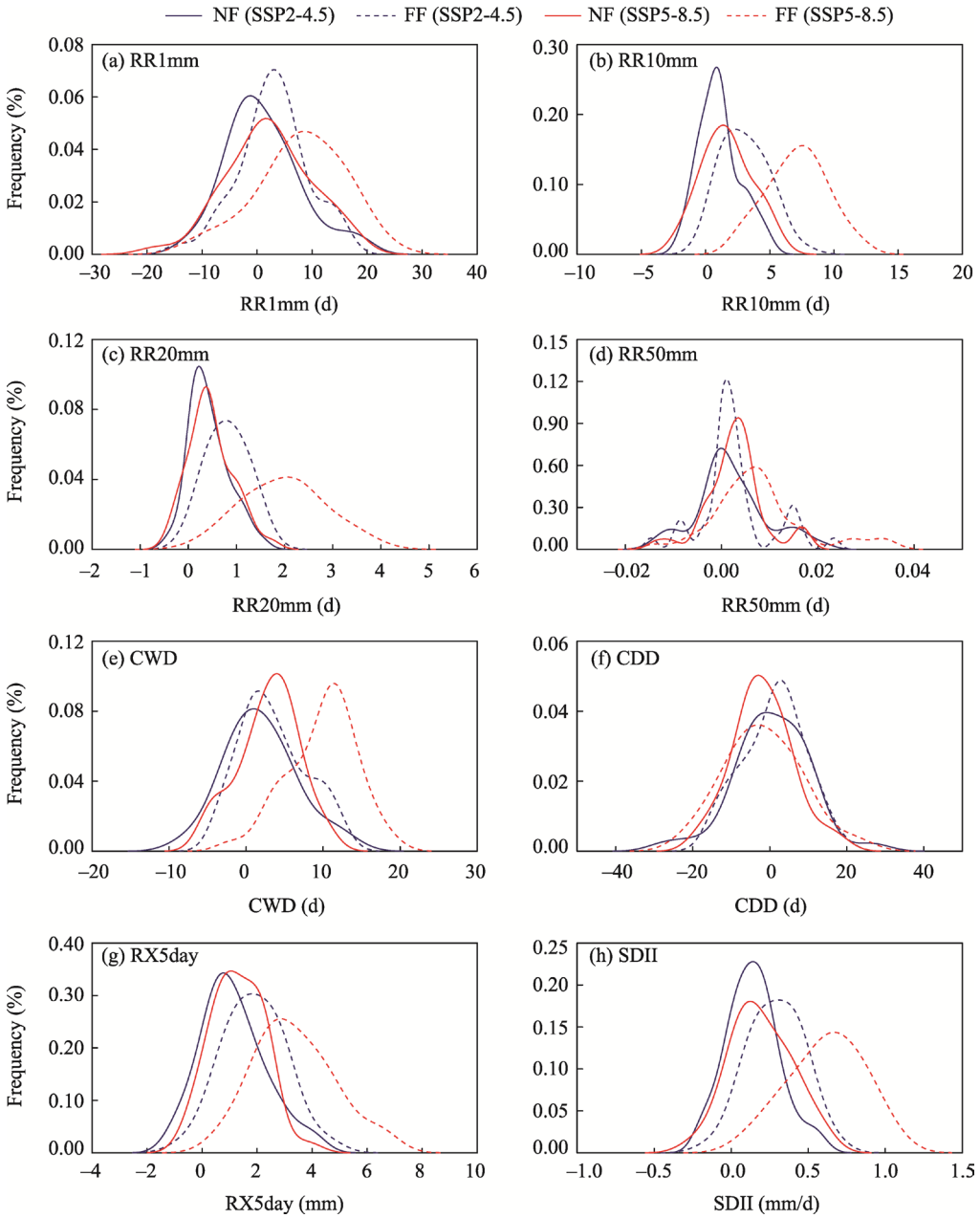

Fig. 8 Estimated probability distribution functions in MMEMs of extreme precipitation indices in the NF and FF periods under SSP2-4.5 and SSP5-8.5 scenarios. (a), RR1mm; (b), RR10mm; (c), RR20mm; (d), RR50mm; (e), CWD; (f), CDD; (g), RX5Day; (h), SDII. The negative values indicate a decreasing trend, while the positive values indicate an increasing trend.

both sides of the tails of the curves. There is a sharp peak of RR50mm around zero, which explains why the probability of a non-existent event remains at zero, leading to a projected shift in the probability distribution of RR50mm, which is anticipated to represent the rarity of these events.

Regarding the distribution of CWD (Fig. 8e), curves produced under the high emission scenario (SSP5-8.5) are tilted towards the right side, projecting values up to 25.00 d, which denotes the increase in the frequency and magnitude of CWD. Conversely, the distribution patterns of CDD reveal some opposite behaviors. For instance, the curves generated under the SSP5-8.5 scenario are skewed towards the left side, and the curves produced under the SSP2-4.5 scenario exhibit a slight shift towards the right side, indicating a decrease in the magnitude of CDD in the FF period (Fig. 8f). In the case of RX5day (Fig. 8g), all curves are skewed towards the right side in the NF and FF periods under the SSP2-4.5 and SSP5-8.5 scenarios, except for the curve in the NF period under the SSP2-4.5 scenario. However, a substantial right shift of RX5day curve is observed in the FF period under the SSP5-8.5 scenario, with a flatter tail and an extreme precipitation value reaching up to 8.50 mm, indicating a significant increase in RX5day in the FF period as compared to the NF period. Likewise, the distribution curves of SDII in the FF period under both scenarios are shifted towards the right side, and the SDII values increase to 1.00 and 1.50 mm/d under the SSP2-4.5 and SSP5-8.5 scenarios, respectively (Fig. 8h).

4.4 Absolute variations in precipitation extremes

The box and whisker plots show the absolute changes in projected precipitation extremes in the NF and FF periods under both scenarios (Fig. 9). The upper and lower limits of the box indicate the 75th and 25th percentile values, respectively. The horizontal line in each box represents the median of the distributions, and the upper and lower whiskers show the 95th and 5th percentile values, respectively (Tang et al., 2021; Ullah et al., 2021b). Some recent studies have also adopted a similar approach to assess the variations in CMIP6 based on projected precipitation over China, East Africa, and Southeast Asia (Ayugi et al., 2021; Supharatid and Nafung, 2021; Xu et al., 2021).

The results of this study indicate that future changes in the median values of all extreme precipitation indices (with an exception of CDD) increase under the high emission scenario (SSP5-8.5) in the NF and FF periods. The reported changes are more pronounced in the FF period since the 25th percentiles are higher than zero. It has been observed from Figure 9a–c that under the high emission scenario (SSP5-8.5), RR1mm, RR10mm, and RR20mm show the maximum values of precipitation extremes up to 24.00, 12.00, and 3.80 d, respectively, in the FF period, which can be noticed from the upper-end whiskers of the boxes. The results suggest that the higher changing rate may be due to the high emission scenario. The analysis of the RR50mm index shows no significant difference in the absolute variability and magnitude of precipitation extremes through the 21st century (Fig. 9d). Moreover, the upper whisker of the box for RR50mm in the FF period under the SSP5-8.5 scenario gives the value up to 0.02 d, which is very close to the value generated under the SSP2-4.5 scenario in the NF period, and the outliers, in this case, are seen to be less probable. Similarly, the median values of CWD produced under the high emission scenario are higher than those under the low emission scenario, indicating an increasing of CWD (>19.00 d) in the FF period (Fig. 9e). In the case of CDD, the box plots depict that the median values of CDD under both scenarios are closer to each other, and no remarkable change is observed (Fig. 9f). Overall, the minimum, maximum, and mean values of projected extreme precipitation indices are consistently increasing under the high emission scenario over the study area during the 21st century, and the region is expected to experience precipitation extremes in the future. Likewise, the projection of the RX5day index exhibits an increasing tendency of median values from the NF period to the FF period under the selected scenarios, giving an increasing value up to 7.00 d in the FF period under the SSP5-8.5 scenario (Fig. 9g). A similar increasing trend is observed for SDII over South Asia, with a sharp difference in the median values projected under the high emission scenario (Fig. 9h). By the end of the 21st century, SDII rises to 1.00 mm/d under the high emission scenario.

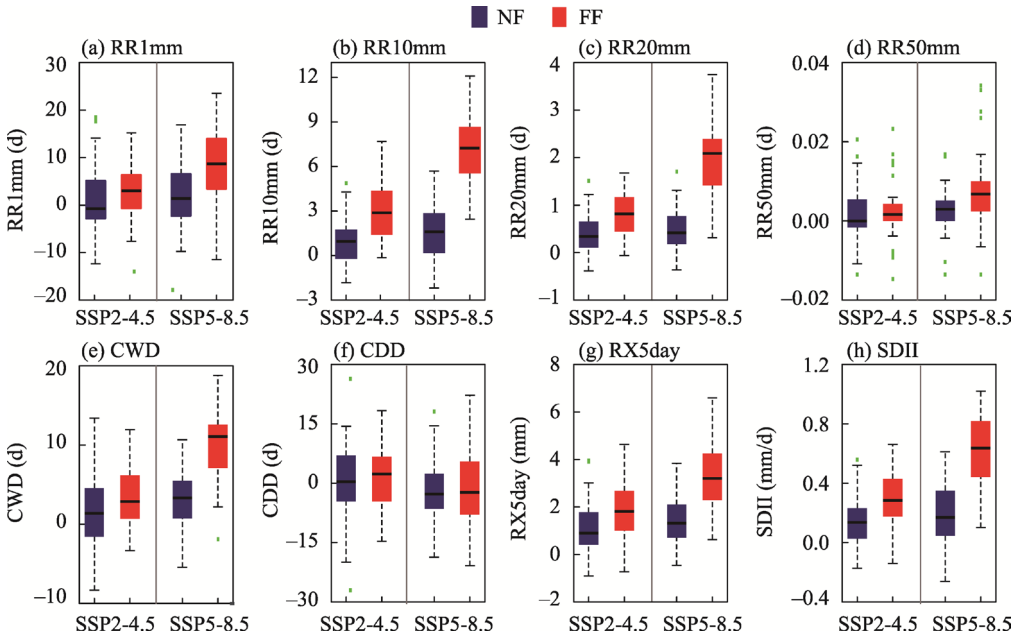

Fig. 9 Box plots showing the changes in MMEMs of extreme precipitation indices in the NF and FF periods under the SSP2-4.5 and SSP5-8.5 scenarios. (a), RR1mm; (b), RR10mm; (c), RR20mm; (d), RR50mm; (e), CWD; (f), CDD; (g), RX5Day; (h), SDII. The upper and lower limits of the box indicate the 75th and 25th percentile values, respectively; the horizontal line in each box represents the median of the distributions; and the upper and lower whiskers show the 95th and 5th percentile values, respectively. The green short lines indicate outliers.

5 Discussion

The results of this study investigate the future changes in the spatiotemporal pattern of precipitation extremes over South Asia, using MMEMs derived from ten CMIP6 GCMs. The trend analyses are based on different spatial and temporal scales, with CMIP6 data being more promising than CMIP3 and CMIP5 data with respect to the start year of future scenarios (i.e., 2021), and using a new set of specifications for emission, concentration, and land-use scenarios (Gidden et al., 2019). In this study, eight extreme precipitation indices were employed to assess the projected precipitation extremes under two emission scenarios (SSP2-4.5 and SSP5-8.5) in the two future time periods (i.e., NF (2020–2060) and FF (2061–2100)) of the 21st century. Some previous studies have remarked on the significance of MMEM over individual models because of the removal of inter-model biases (e.g., Ullah et al., 2022b). In addition, MMEM also provides clear identification of signals of interest, as averaging the climatic models also gives a natural variability of the study area (Sylla et al., 2018; Zhang et al., 2018; Almazroui et al., 2020; Akinsanola et al., 2021; Lun et al., 2021). Many other studies also suggest the importance of MMEM, as it replicates precipitation extremes compared to the individual climatic models (e.g., Zhu et al., 2020; Fischer et al., 2021). Given the importance of MMEM, we assessed future changes in precipitation extremes in South Asia based on both individual climatic models and respective MMEMs.

The results indicate that South Asia is expected to experience precipitation extremes in the FF period (2061–2100) relative to the NF period (2021–2060) under the high emission scenario (SSP5-8.5). Figures 2 and 3 portray the temporal evolution of future precipitation extremes generated by the individual climatic models and their MMEMs, describing the increase in the intensity of precipitation extremes in the FF period. For instance, the MMEMs of RR1mm (3.00–9.00 d), RR10mm (3.00–7.00 d), RR20mm (0.90–2.00 d), CWD (4.00–10.00 d), and SDII (0.90–6.00 mm/d) demonstrate a significant increase in precipitation extremes as compared to other indices. On the other hand, the CDD index reveals a decreasing trend of precipitation

extremes under the high emission scenario. These results follow the IPCC-AR6, which demonstrates an increase in projected precipitation extremes through the 21st century in South Asia (IPCC, 2021). According to the spatial distribution of projected extreme precipitation indices (Figs. 4–7), it has been observed that MMEMs can capture the spatial characteristics of precipitation extremes over South Asia, showing a substantial increase in the southeastern part as compared to the western part in the FF period.

These results are in line with the recent research of Almazroui et al. (2020), who used CMIP6 models to project precipitation changes over South Asia, and found an increase in annual mean precipitation by 10%–50% under the SSP5-8.5 scenario towards the end of the century. Simultaneously, the kernel density estimation also justifies the increase in the frequency of precipitation extremes in the FF period under the SSP5-8.5, with RR1mm values up to 35.00 d and CWD values up to 25.00–35.00 d (Fig. 8). Similarly, the box and whisker plots demonstrate the intensification of RR10mm, RR20mm, CWD, RX5day, and SDII over South Asia in the FF period (Fig. 9). The IPCC-AR6 also supports the increase in mean precipitation from the near-term (2021–2040) to the long-term (2081–2100) in South Asia, and these results are based on 24 CMIP6 GCMs under the SSP2-4.5 scenario (IPCC, 2021). However, in all analyses of this study, RR50mm exhibits uncertainty in its occurrence and therefore, its temporal and spatial distribution gives no remarkable change under the selected scenarios. According to the kernel density estimation and box and whisker plots, there is a slightly decreasing tendency of CDD in the FF period under the SSP5-8.5 scenario, indicating a wetting trend in the future under the high emission scenario.

Overall, there is an increase in precipitation extremes in South Asia in the FF period under the high emission scenario, and this observation is in agreement with the existing studies (Ogata et al., 2014; Sharmila et al., 2015; Jena et al., 2016; Kitoh, 2017; Woo et al., 2018; Scoccimarro and Gualdi, 2020; Almazroui et al., 2021; Shrestha et al., 2021), which were conducted by using CMIP3, CMIP5, and CMIP6 GCMs. However, the spatial distribution of projected extreme precipitation indices (Figs. 4–7) indicates that the increasing tendency of precipitation extremes is more significant in the eastern part of South Asia, as compared to the western part; these findings are consistent with the previous studies (Almazroui et al., 2020; Zhai et al., 2020). Changing precipitation extremes from the NF period to the FF period suggests the need for careful analysis of current water and agriculture management practices and demand for making new strategies, planning, and adaptive measures that are flexible enough to adopt to the changing climatic behaviors and make the system resilient to new climatic trends. In addition, the robust increase of precipitation extremes in response to the SSP5-8.5 scenario indicates the sensitivity of this region towards high greenhouse gas emissions, which can be minimized by limiting the emissions of greenhouse gases.

The above results indicate that South Asia is prone to experience wet conditions in the future. This climatic condition will offer an opportunity to enhance agricultural production and ensure food security in this region; however, the lack of appropriate water resources management can result in flooding, which is catastrophic for agricultural production, human livelihoods, and the sustainable development of ecosystems. Moreover, this study serves to identify certain parts of the region that could be sensitive to climatic vulnerabilities for food and water security. The changing precipitation pattern can alter the planting schedule, soil characteristics, and crop types. In other words, climate change can alter certain agriculture practices in a region that is entirely dependent on water availability, and trigger food security issues. Thus, systemically sustainable development can mitigate food insecurity and vulnerability. Therefore, the current analyses highlight the need to understand the changing climatic pattern of South Asia to develop appropriate adaptation measures to minimize the associated risks.

6 Conclusions

The present study examined the expected changes in future precipitation extremes over South

Asia by employing ten CMIP6 GCMs and their MMEMs. A total of eight extreme precipitation indices were analyzed to explore the spatiotemporal evolution, frequency, and magnitude of projected precipitation extremes in two future time periods (NF (2021–2060) and FF (2061–2100)) under two emission scenarios (SSP2-4.5 and SSP5-8.5). The temporal distribution of extreme precipitation indices suggests a significant increase in the occurrence of RR1mm, RR10mm, RR20mm, CWD, and SDII in the FF period under the SSP2-4.5 and SSP5-8.5 scenarios. This implies that the intensification of precipitation extremes will be higher under the high emission scenario (SSP5-8.5) compared with the low emission scenario (SSP2-4.5).

The spatial distribution results clearly show that the eastern part of South Asia will have to be more affected by precipitation extremes in the FF period under the SSP5-8.5 scenario than the western part of South Asia. The estimated kernel density under both scenarios reflects the projected results of extreme precipitation indices, which show the increases in the frequency and amplitude of RR1mm, RR10mm, RR20mm, CWD, RX5day, and SDII towards the end of the century. From the results of absolute variations it can be seen that the distribution of the median varies with different indices, and the median increases with large amplitudes for RR1mm, RR10mm, RR20mm, CWD, RX5day, and SDII indices in the FF period under the SSP5-8.5 scenario. The CDD index shows a consistent trend across all analyses, with the occurrence, magnitude, and frequency gradually declining over time. Similarly, the RR50mm index does not reveal a significant trend in its spatiotemporal distribution over the study area. Overall, precipitation is increasing from the NF period to the FF period under the high emission scenario, suggesting that South Asia is expected to experience severe precipitation in the future, which will alleviate water resource shortage and promote agricultural-related activities, while magnify the risk of water resources management in this region. The results presented here give significant implications for the analysis of precipitation extremes in this region and therefore, offering corresponding policymakers with reference to prepare necessarily adaptive measures for minimizing the climatic-induced risks.

Acknowledgements

The study was supported by the National Natural Science Foundation of China (42130405), the Innovative and Entrepreneurial Talent Program of Jiangsu Province (R2020SC04), the Strategic Priority Research Program of the Chinese Academy of Sciences (XDA2006030201), and the Research Fund for International Young Scientists of the National Natural Science Foundation of China (42150410381).

References

Abbas A, Ullah S, Ullah W, et al. 2022. Evaluation and projection of precipitation in Pakistan using the Coupled Model Intercomparison Project Phase 6 model simulations. International Journal of Climatology, 42(13): 6665–6684.

Abbas F, Rehman I, Adrees M, et al. 2018. Prevailing trends of climatic extremes across Indus-Delta of Sindh-Pakistan. Theoretical and Applied Climatology, 131(3–4): 1101–1117.

Ahmed K, Shahid S, Nawaz N. 2018. Impacts of climate variability and change on seasonal drought characteristics of Pakistan. Atmospheric Research, 214: 364–374.

Ahmed K, Shahid S, Wang X J, et al. 2019. Spatiotemporal changes in aridity of Pakistan during 1901–2016. Hydrology and Earth System Sciences, 23(7): 3081–3096.

Akinsanola A A, Ongoma V, Kooperman G J. 2021. Evaluation of CMIP6 models in simulating the statistics of extreme precipitation over Eastern Africa. Atmospheric Research, 254: 105509 , doi: 10.1016/j.atmosres.2021.105509.

Alashan S. 2020. Combination of modified Mann-Kendall method and Şen innovative trend analysis. Engineering Reports, 2(3): e12131, doi: 10.1002/eng2.12131.

Allen M R, Ingram W J. 2002. Constraints on future changes in climate and the hydrologic cycle. Nature, 419(6903): 224–232.

Almazroui M, Kamil S, Ammar K, et al. 2016. Climatology of the 500-hPa Mediterranean storms associated with Saudi Arabia wet season precipitation. Climate Dynamics, 47(9–10): 3029–3042.

Almazroui M, Raju P V S, Yusef A, et al. 2018. Simulation of extreme rainfall event of November 2009 over Jeddah, Saudi Arabia: the explicit role of topography and surface heating. Theoretical and Applied Climatology, 132(1–2): 89–101.

Almazroui M, Saeed S, Saeed F, et al. 2020. Projections of precipitation and temperature over the South Asian Countries in CMIP6. Earth Systems and Environment, 4: 297–320.

Almazroui M, Islam M N, Saeed F, et al. 2021. Projected changes in temperature and precipitation over the United States, Central America, and the Caribbean in CMIP6 GCMs. Earth Systems and Environment, 5: 1–24.

Andrijevic M, Byers E, Mastrucci A, et al. 2021. Future cooling gap in shared socioeconomic pathways. Environmental Research Letters, 16(9): 094053, doi: 10.1088/1748-9326/ac2195.

Ayugi B, Dike V, Ngoma H, et al. 2021. Future changes in precipitation extremes over East Africa based on CMIP6 models. Water, 13(17): 2358, doi: 10.3390/w13172358.

Azad A K, Hossain K M, Nasreen M. 2013. Flood-induced vulnerabilities and problems encountered by women in northern Bangladesh. International Journal of Disaster Risk Science, 4: 190–199.

Bandara J S, Cai Y Y. 2014. The impact of climate change on food crop productivity, food prices and food security in South Asia. Economic Analysis and Policy, 44(4): 451–465.

Bhatti A S, Wang G J, Ullah W, et al. 2020. Trend in extreme precipitation indices based on long term *in situ* precipitation records over Pakistan. Water, 12(3): 797, doi: 10.3390/w12030797.

Blain G C. 2013. The modified Mann-Kendall test: on the performance of three variance correction approaches. Bragantia, 72(4): 416–425.

Chen F H, Chen J H, Huang W, et al. 2019. Westerlies Asia and monsoonal Asia: Spatiotemporal differences in climate change and possible mechanisms on decadal to sub-orbital timescales. Earth-Science Reviews, 192: 337–354.

Chen H P, Sun J Q. 2019. Increased population exposure to extreme droughts in China due to 0.5°C of additional warming. Environmental Research Letters, 14(6): 064011, doi: 10.1088/1748-9326/ab072e.

Chen X L, Zhou T J. 2015. Distinct effects of global mean warming and regional sea surface warming pattern on projected uncertainty in the South Asian summer monsoon. Geophysical Research Letters, 42(21): 9433–9439.

Chen Z M, Zhou T J, Zhang L X, et al. 2020. Global land monsoon precipitation changes in CMIP6 projections. Geophysical Research Letters, 47(14): e2019GL086902, doi: 10.1029/2019GL086902.

Christensen O B, Christensen J H. 2004. Intensification of extreme European summer precipitation in a warmer climate. Global and Planetary Change, 44(1–4): 107–117.

Dimri A P, Niyogi D, Barros A P, et al. 2015. Western disturbances: A review. Reviews of Geophysics, 53(2): 225–246.

Endo H, Kitoh A. 2014. Thermodynamic and dynamic effects on regional monsoon rainfall changes in a warmer climate. Geophysical Research Letters, 41(5): 1704–1710.

Filippi L, Palazzi E, von Hardenberg J, et al. 2014. Multidecadal variations in the relationship between the NAO and winter precipitation in the Hindu Kush-Karakoram. Journal of Climate, 27(20): 7890–7902.

Fischer E M, Sippel S, Knutti R. 2021. Increasing probability of record-shattering climate extremes. Nature Climate Change, 11(8): 689–695.

Fróna D, Szenderák J, Harangi-Rákos M. 2021. Economic effects of climate change on global agricultural production. Nature Conservation, 44: 117–139.

Gidden M J, Riahi K, Smith S J, et al. 2019. Global emissions pathways under different socioeconomic scenarios for use in CMIP6: A dataset of harmonized emissions trajectories through the end of the century. Geoscientific Model Development, 12(4): 1443–1475.

Gupta V, Jain M K. 2018. Investigation of multi-model spatiotemporal mesoscale drought projections over India under climate change scenario. Journal of Hydrology, 567: 489–509.

Hamed K H, Rao A R. 1998. A modified Mann-Kendall trend test for autocorrelated data. Journal of Hydrology, 204(1–4): 182–196.

Hanf F S, Annamalai H, Rinke A, et al. 2017. South Asian summer monsoon breaks: Process-based diagnostics in HIRHAM5. Journal of Geophysical Research: Atmospheres, 122(9): 4880–4902.

Held I M, Soden B J. 2006. Robust responses of the hydrological cycle to global warming. Journal of Climate, 19(21): 5686–5699.

Herring S C, Christidis N, Hoell A, et al. 2021. Explaining extreme events of 2019 from a climate perspective. Bulletin of the American Meteorological Society, 102(1): S1–S115.

Hulme M. 2016. 1.5°C and climate research after the Paris Agreement. Nature Climate Change, 6(3): 222–224.

Hunt K M R, Turner A G, Shaffrey L C. 2018. The evolution, seasonality and impacts of western disturbances. Quarterly Journal of the Royal Meteorological Society, 144(710): 278–290.

Hussain M, Liu G J, Yousaf B, et al. 2018. Regional and sectoral assessment on climate-change in Pakistan: Social norms and indigenous perceptions on climate-change adaptation and mitigation in relation to global context. Journal of Cleaner

Production, 200: 791–808.

Immerzeel W W, Wanders N, Lutz A F, et al. 2015. Reconciling high-altitude precipitation in the upper Indus basin with glacier mass balances and runoff. Hydrology and Earth System Sciences, 19(11): 4673–4687.

IPCC. 2014. Climate Change 2014: The Physical Science Basis. Working Group I Contribution to the Fifth Assessment Report of the Intergovernmental Panel on Climate Change. Cambridge: Cambridge University Press.

IPCC. 2021. Climate Change 2021: The Physical Science Basis. Contribution of Working Group I to the Sixth Assessment Report of the Intergovernmental Panel on Climate Change. In: Masson-Delmotte V, Zhai P, Pirani A, et al. Cambridge and New York: Cambridge University Press.

Iqbal M A, Penas A, Cano-Ortiz A, et al. 2016. Analysis of recent changes in maximum and minimum temperatures in Pakistan. Atmospheric Research, 168: 234–249.

Jena P, Azad S, Rajeevan M N. 2016. CMIP5 projected changes in the annual cycle of Indian monsoon rainfall. Climate, 4(1): 14, doi: 10.3390/cli4010014.

Jiang R G, Wang Y P, Xie J C, et al. 2019. Assessment of extreme precipitation events and their teleconnections to El Niño Southern Oscillation, a case study in the Wei River Basin of China. Atmospheric Research, 218: 372–384.

Joshi S, Kar S C. 2018. Mechanism of ENSO influence on the South Asian monsoon rainfall in global model simulations. Theoretical and applied climatology, 131(3–4): 1449–1464.

Khan I, Waqas T, Samiullah, et al. 2020. Precipitation variability and its trend detection for monitoring of drought hazard in northern mountainous region of Pakistan. Arabian Journal of Geosciences, 13(15): 698, doi: 10.1007/s12517-020-05700-4.

Khan I, Ali A, Waqas A, et al. 2022. Investing in disaster relief and recovery: A reactive approach of disaster management in Pakistan. International Journal of Disaster Risk Reduction, 75: 1–10.

Kitoh A. 2017. The Asian monsoon and its future change in climate models: A review. Journal of the Meteorological Society of Japan, 95(1): 7–33.

Kripalani R H, Oh J H, Kulkarni A, et al. 2007. South Asian summer monsoon precipitation variability: Coupled climate model simulations and projections under IPCC AR4. Theoretical and Applied Climatology, 90: 133–159.

Latif M, Syed F S, Hannachi A. 2017. Rainfall trends in the South Asian summer monsoon and its related large-scale dynamics with focus over Pakistan. Climate Dynamics, 48(11): 3565–3581.

Lehtonen H S, Aakkula J, Fronzek S, et al. 2021. Shared socioeconomic pathways for climate change research in Finland: co-developing extended SSP narratives for agriculture. Regional Environmental Change, 21(1): 7, doi: 10.1007/s10113-020-01734-2.

Li R Q, Lv S H, Han B, et al. 2017. Projections of South Asian summer monsoon precipitation based on 12 CMIP5 models. International Journal of Climatology, 37(1): 94–108.

Li W, Jiang Z, Xu J, et al. 2016. Extreme precipitation indices over China in CMIP5 models. Part II: probabilistic projection. Journal of Climate, 29(24): 8989–9004.

Lun Y R, Liu L, Cheng L, et al. 2021. Assessment of GCMs simulation performance for precipitation and temperature from CMIP5 to CMIP6 over the Tibetan Plateau. International Journal of Climatology, 41(7): 3994–4018.

Marotzke J, Jakob C, Bony S, et al. 2017. Climate research must sharpen its view. Nature Climate Chang, 7(2): 89–91.

Medina S, Houze R A, Kumar A, et al. 2010. Summer monsoon convection in the Himalayan region: terrain and land cover effects. Quarterly Journal of the Royal Meteorological Society, 136(648): 593–616.

Mishra V, Bhatia U, Tiwari A D. 2020. Bias-corrected climate projections for South Asia from Coupled Model Intercomparison Project-6. Scientific Data, 7(1): 338, doi: 10.1038/s41597-020-00681-1.

Nikulin G, Lennard C, Dosio A, et al. 2018. The effects of 1.5 and 2 degrees of global warming on Africa in the CORDEX ensemble. Environmental Research Letters, 13(6): 065003, doi: 10.1088/1748-9326/aab1b1.

Nooni I K, Hagan D F T, Wang G J, et al. 2021. Spatiotemporal characteristics and trend analysis of two evapotranspiration-based drought products and their mechanisms in sub-Saharan Africa. Remote Sensing, 13(3): 533, doi: 10.3390/rs13030533.

Ogata T, Ueda H, Inoue T, et al. 2014. Projected future changes in the Asian monsoon: A comparison of CMIP3 and CMIP5 model results. Journal of the Meteorological Society of Japan, 92(3): 207–225.

Ongoma V, Chen H S, Gao C J, et al. 2018. Future changes in climate extremes over Equatorial East Africa based on CMIP5 multimodel ensemble. Natural Hazards, 90(2): 901–920.

Papalexiou S M, Montanari A, 2019. Global and regional increase of precipitation extremes under global warming. Water Resources Research, 55(6): 4901–4914.

Phillips N. 2020. Climate change made Australia's devastating fire season 30% more likely. Nature, doi: 10.1038/D41586-020-00627-Y.

Rahman G, Atta-ur-Rahman, Samiullah, et al. 2018. Spatial and temporal variation of rainfall and drought in Khyber

Pakhtunkhwa Province of Pakistan during 1971–2015. Arabian Journal of Geosciences, 11(3): 46, doi: 10.1007/s12517-018-3396-7.

Ramachandran S, Kedia S. 2013. Aerosol optical properties over South Asia from ground-based observations and remote sensing: a review. Climate, 1(3): 84–119.

Rasmussen K L, Hill A J, Toma V E, et al. 2015. Multiscale analysis of three consecutive years of anomalous flooding in Pakistan. Quarterly Journal of the Royal Meteorological Society, 141(689): 1259–1276.

Ren Y Y, Ren G Y, Sun X B, et al. 2017. Observed changes in surface air temperature and precipitation in the Hindu Kush Himalayan region over the last 100-plus years. Advances in Climate Change Research, 8(3): 148–156.

Riahi K, van Vuuren D P, Kriegler E, et al. 2016. The Shared Socioeconomic Pathways and their energy, land use, and greenhouse gas emissions implications: An Overview. Global Environmental Change, 42: 153–168.

Scoccimarro E, Gualdi S. 2020. Heavy daily precipitation events in the CMIP6 worst-case scenario: Projected twenty-first-century changes. Journal of Climate, 33(17): 7631–7642.

Sen P K. 1968. Estimates of the regression coefficient based on Kendall's Tau. Journal of the American Statistical Association, 63: 1379–1389, doi: 10.1080/01621459.1968.10480934.

Sharmila S, Joseph S, Sahai A K, et al. 2015. Future projection of Indian summer monsoon variability under climate change scenario: An assessment from CMIP5 climate models. Global and Planetary Change, 124: 62–78.

Shen L, Wen J, Zhang Y, et al. 2022 Changes in population exposure to extreme precipitation in the Yangtze River Delta, China. Climate Services, 27: 100317, do: 10.1016/j.cliser.2022.100317.

Shiu C J, Liu S C, Fu C B, et al. 2012. How much do precipitation extremes change in a warming climate? Geophysical Research Letters, 39(17): L17707, doi: 10.1029/2012GL052762.

Shrestha S, Bae D H, Hok P, et al. 2021. Future hydrology and hydrological extremes under climate change in Asian river basins. Scientific Reports, 11(1): 17089, doi: 10.1038/s41598-021-96656-2.

Sillmann J, Stjern C W, Myhre G, et al. 2017. Slow and fast responses of mean and extreme precipitation to different forcing in CMIP5 simulations. Geophysical Research Letters, 44(12): 6383–6390.

Sun X B, Ren G Y, Shrestha A B, et al. 2017. Changes in extreme temperature events over the Hindu Kush Himalaya during 1961–2015. Advances in Climate Change Research, 8(3): 157–165.

Supharatid S, Nafung J, 2021. Projected drought conditions by CMIP6 multimodel ensemble over Southeast Asia. Journal of Water and Climate Change, 12(7): 3330–3354.

Syed A, Zhang J, Rousta I, et al. 2022. Statistical analysis of precipitation variations and its forecasting in Southeast Asia using remote sensing images. Frontiers in Environmental Science, 10, doi: 10.3389/fenvs.2022.832427.

Sylla M B, Faye A, Giorgi F, et al. 2018. Projected heat stress under 1.5°C and 2°C global warming scenarios creates unprecedented discomfort for humans in West Africa. Earth's Future, 6(7): 1029–1044.

Tabari H. 2020. Climate change impact on flood and extreme precipitation increases with water availability. Scientific Reports, 10(1): 13768, doi: 10.1038/s41598-020-70816-2.

Thibeault J M, Seth A. 2014. Changing climate extremes in the Northeast United States: observations and projections from CMIP5. Climate Change, 127: 273–287.

Turner A G, Annamalai H. 2012. Climate change and the South Asian summer monsoon. Nature Climate Change, 2(8): 587–595.

Ullah S, You Q L, Ullah W, et al. 2018. Observed changes in precipitation in China-Pakistan economic corridor during 1980–2016. Atmospheric Research, 210: 1–14.

Ullah S, You Q L, Ullah W, et al. 2019a. Observed changes in temperature extremes over China-Pakistan Economic Corridor during 1980–2016. International Journal of Climatology, 39(3): 1457–1475.

Ullah S, You Q L, Ullah W, et al. 2019b. Daytime and nighttime heat wave characteristics based on multiple indices over the China–Pakistan economic corridor. Climate Dynamics, 53(9–10): 6329–6349.

Ullah S, You Q L, Zhang Y Q, et al. 2020. Evaluation of CMIP5 models and projected changes in temperatures over South Asia under global warming of 1.5°C, 2°C, and 3°C. Atmospheric Research, 246: 105122, doi: 10.1016/J.ATMOSRES.2020.105122.

Ullah S, You Q L, Chen D L, et al. 2022a. Future population exposure to daytime and nighttime heat waves in South Asia. Earth's Future, 10(5): e2021EF002511, doi: 10.1029/2021EF002511.

Ullah S, You Q L, Wang G, et al. 2022b. Characteristics of human thermal stress in South Asia during 1981–2019. Environmental Research Letters, 17: 104018, doi:10.1088/1748-9326/ac8fa6.

Ullah W, Wang G J, Gao Z Q, et al. 2021a. Observed linkage between Tibetan Plateau soil moisture and South Asian summer precipitation and the possible mechanism. Journal of Climate, 34(1): 361–377.

Ullah W, Wang G J, Lou D, et al. 2021b. Large-scale atmospheric circulation patterns associated with extreme monsoon

precipitation in Pakistan during 1981–2018. Atmospheric Research, 253: 105489, doi: 10.1016/J.ATMOSRES.2021.105489.

Vecchi G A, Soden B J, Wittenberg A T, et al. 2006. Weakening of tropical Pacific atmospheric circulation due to anthropogenic forcing. Nature, 441(7089): 73–76.

Watterson I, Rafter T. 2017. The distribution of daily rainfall in Australia and simulated future changes. Journal of Southern Hemisphere Earth System Science, 67(3): 160–180.

Wen X H, Wu X Q, Gao M. 2017. Spatiotemporal variability of temperature and precipitation in Gansu Province (Northwest China) during 1951–2015. Atmospheric Research, 197: 132–149.

WMO (World Meteorological Organization). 2021. WMO atlas of mortality and economic losses from weather, climate and water extremes (1970–2019) (WMO-No. 1267). Geneva, Switzerland. [2022-10-14]. https://library.wmo.int/index.php?lvl=notice_display&id=21930#.Y0uvcnbP2Uk.

Woo S, Singh G P, Oh J H, et al. 2018. Projected changes in summer precipitation over East Asia with a high-resolution atmospheric general circulation model during 21st century. International Journal of Climatology, 38(12): 4610–4631.

Wu S H, Liu L L, Liu Y H, et al. 2019. The Belt and Road: Geographical pattern and regional risks. Journal of Geographical Sciences, 29(4): 483–495.

Xu L, Zheng C L, Ma Y. 2021. Variations in precipitation extremes in the arid and semi-arid regions of China. International Journal of Climatology, 41(3): 1542–1554.

Yadav S S, Lal R. 2018. Vulnerability of women to climate change in arid and semi-arid regions: The case of India and South Asia. Journal of Arid Environments, 149: 4–17.

Yu Y, You Q L, Zuo Z, et al. 2023. Compound climate extremes in China: Trends, causes, and projections, 286: 106675, doi: 10.1016/j.atmosres.2023.106675.

Zhai J Q, Mondal S K, Fischer T, et al. 2020. Future drought characteristics through a multi-model ensemble from CMIP6 over South Asia. Atmospheric Research, 246: 105111, doi: 10.1016/j.atmosres.2020.105111.

Zhang X B, Alexander L, Hegerl G C, et al. 2011. Indices for monitoring changes in extremes based on daily temperature and precipitation data. Wiley Interdisciplinary Reviews: Climate Change, 2(6): 851–870.

Zhang Y Q, You Q L, Chen C C, et al. 2018. Evaluation of downscaled CMIP5 coupled with VIC Model for flash drought simulation in a humid subtropical basin, China. Journal of Climate, 31(3): 1075–1090.

Zhou S J, Huang G, Huang P. 2018. Changes in the East Asian summer monsoon rainfall under global warming: moisture budget decompositions and the sources of uncertainty. Climate Dynamics, 51(4): 1363–1373.

Zhu H H, Jiang Z H, Li J, et al. 2020. Does CMIP6 inspire more confidence in simulating climate extremes over China? Advances in Atmospheric Sciences, 37(10): 1119–1132.